

Effect of Linear Heat Input on the Morphology and Mechanical Properties of Ti-6Al-4V Welded Using a CO₂ Laser

Khorrām, A., Jafari, A. & Moradi, M.

Author post-print (accepted) deposited by Coventry University's Repository

Original citation & hyperlink:

Khorrām, A, Jafari, A & Moradi, M 2018, 'Effect of Linear Heat Input on the Morphology and Mechanical Properties of Ti-6Al-4V Welded Using a CO₂ Laser', *Lasers in Engineering*, vol. 40, no. 1-3, pp. 49-64.

<http://www.oldcitypublishing.com/journals/lie-home/lie-issue-contents/lie-volume-40-number-1-3-2018/lie-40-1-3-p-49-64/>

ISSN 0898-1507

ESSN 1029-029X

Publisher: Old City Publishing

Copyright © and Moral Rights are retained by the author(s) and/ or other copyright owners. A copy can be downloaded for personal non-commercial research or study, without prior permission or charge. This item cannot be reproduced or quoted extensively from without first obtaining permission in writing from the copyright holder(s). The content must not be changed in any way or sold commercially in any format or medium without the formal permission of the copyright holders.

This document is the author's post-print version, incorporating any revisions agreed during the peer-review process. Some differences between the published version and this version may remain and you are advised to consult the published version if you wish to cite from it.

Effect of linear heat input on morphology and mechanical properties of Ti-6Al-4V welded using a CO₂ laser

A. Khorram^{a,*}, A. jafari^b, M. Moradi^c

^a *Department of Mechanical Engineering, KNToosi University of Technology, P.O. Box 19395-1999, Tehran, Iran*

^b *Faculty of Engineering and High Technology, Iran University of Industries and Mines (IUIM), Tehran, Iran*

^c *Department of Mechanical Engineering, Faculty of Engineering, Malayer University*

Corresponding author: alikhorram@ymail.com, akhorram@mail.kntu.ac.ir

ABSTRACT

Butt welds were carried out on Ti-6Al-4V sheets with thickness 1.7 mm using a 2.2 KW CO₂ laser welding. The effect of linear heat input on the joint geometry, microstructure and mechanical properties was investigated. The welding process efficiency (E) and the ratio of root width to top width (R_w) were used to evaluate the joints. The results showed that fully penetrated joints were achieved at linear heat input of greater than 4 J/mm. Metallographic observations showed that fusion zone consists of acicular α' phase within prior coarse β grains. Increasing linear heat input causes to change the martensitic phase from an acicular like to plate like morphology. Also, the prior β grain size increases because longer time exists for β grain coarsening. The micro hardness values in the fusion zone decrease with increasing the linear heat input. This phenomenon can be attributed to decrease of martensitic phase formation in the fusion zone. The ultimate tensile strength of the joints ranges from 624 MPa to 1002 MPa at room temperature.

Keywords: CO₂ laser, Laser welding, Ti-6Al-4V alloy, Linear heat input, Microstructure, Mechanical properties

1 INTRODUCTION

Laser beam is coherent, monochromatic and collimated. It focuses on a small area and creates high-power density on the material surface and results in producing a keyhole during welding. [1]

Ti-6Al-4V alloy is a dual phase alloys consisting of α and β phases. It is currently the most common among all titanium alloys and widely used in industries. High strength to weight ratio, good corrosion resistance and suitable adaptability to human body lead to its application in medical, chemistry and aerospace industries. [2]

Many joining methods have been used to perform titanium assemblies [3-7]. Laser welding is one of the most suitable joining methods for this purpose. Some research about the influence of laser welding parameters on the bead geometry, microstructure and mechanical properties of Ti-6Al-4V laser welds has been accomplished. Influence of pulse laser welding parameters (pulse energy, pulse duration, pulse frequency, welding speed and focal point position) on Porosity and microstructure of Ti-6Al-4V welded joints was investigated by Gao et al. [7]. Their aim was to provide a method of porosity elimination. Casalino et al. [8] used a high brightness Yb fiber laser for obtaining full penetration welding of 2 mm thick Ti-6Al-4V plates in butt configuration. They investigated the influence of different welding conditions on the bead morphology, metallurgy and mechanical properties. The work of Xu et al. [9] showed the phase transformation is affected by the cooling rate through laser welding speed. A higher welding speed of 1.6 to 2.0 m/min produced more martensite α' and less retained β in the welds. 1.4 m/min welding speed produced small amounts of α , besides the martensite α' . Casalino et al. [10] investigated butt-welding of Ti-6Al-4V alloy sheet using Taguchi approach. They used a continuous wave CO₂ laser with a maximum power 2.5 kW and a diode laser with a maximum power of 2.2 kW for joining Ti-6Al-4V alloy sheet. Xiansheng et al. [11] studied the effects of the Nd:YAG laser welding parameters (laser

power, welding speed, defocusing amount and shield gas) and then proposed a novel application of Taguchi's matrix method to optimize the laser seal welding of thin titanium shell. Li et al. [12] showed that welding parameters affect on weld geometry during high-power laser welding of thick plate. Caiazzo et al. [13] investigated the influence of various different cooling speed rates and input energy levels on the melted and re-solidified zone. They used two covering gases (He or Ar) with different welding nozzles, gas pressure and flow rates in order to quantitatively evaluate the influence of the different gases on the mechanical characteristics of the welded joint. Akman et al. [14] employed pulsed Nd: YAG laser to investigate the effect of pulse energy and pulse duration on the quality of 3 mm thick Ti-6Al-4V seam welds. They reported that the ratio between the pulse energy and pulse duration is the most important parameter in defining the penetration depth. The effects of laser parameters (welding speed and laser power) on the weld quality of Ti-6Al-4V sheets autogenously laser beam welded in butt configuration using Nd: YAG laser was studied by Squillace et al. [15]. Cao et al. [16] investigated the effect of welding speed on surface morphology and shape, welding defect, microstructure, hardness and tensile properties of annealed Ti-6Al-4V laser welds. The work of them showed that high-power Nd:YAG laser welding is a suitable method for joining of Ti-6Al-4V alloy sheets with 1 and 2 mm thickness and joints without or with minor cracks, porosity and shape defects can be obtained. Ahn et al. [17] focused on the effect of welding parameters including laser power, welding speed and beam focal position on the weld microstructure, bead profile and weld quality of Ti-6Al-4V alloy. Then, they identified optimum range of welding parameters which produced welds without cracking and porosity. Kashaev et al. [18] performed Nd:YAG single-sided laser beam welding process for Ti-6Al-4V butt joints and T-joints to investigate the effect of welding parameters on weld morphology and mechanical properties of joints.

They obtained joints with regular shapes, without visible cracks, pores, and geometrical defects.

In this paper, CO₂ laser butt welding was carried out on Ti-6Al-4V sheets with thickness 1.7 mm. The influence of linear heat input on the bead morphology, microstructure and mechanical properties of Ti-6Al-4V laser welds was investigated. The welded cross sections of the joints were characterized by using three geometric parameters: penetration depth (P_d), fusion zone width (W_{FZ}) and fusion zone area (A_{FZ}). The welding process efficiency (E) and the ratio of root width to top width (R_w) were used to evaluate the joints. The microstructural characterization of Ti-6Al-4V alloy and welded samples were observed by optical microscope (OM) and scanning electron microscopy (SEM) equipped with an energy dispersive x-ray spectroscopy (EDS). Tensile tests at room temperature and micro hardness tests were conducted to assess the mechanical properties of joints.

2 EXPERIMENTAL PROCEDURE

1.7 mm thick Ti-6Al-4V alloy with chemical composition presented in Table 1 was used as base metal. The size of sheets was 85 mm long \times 35 mm width. Prior to laser welding process the parts were grinded in order to allow a very narrow air gap between sheet edges and then cleaned with acetone.

A 2.2 KW maximum output continuous CO₂ laser (Optimo model, provided by OPTIMA Industries) was used to weld the butt joints. Argon gas with flow rate of 20 l/min was used as shielding gas at the weld bead and the weld root of the samples to protect the molten pool from oxidation. The focal point was positioned at 0.5 mm under the top surface. Several preliminary experiments were performed to find the suitable values of process parameters. Absence of visible welding defects and at least half depth penetration were the criteria of choosing the parameters. Table 2 shows the parameters variables used in this study and the optimal process parameter.

In our previous studies [19, 20], the effect of laser parameters on the weld geometry and optimization of bead geometry using response surface methodology were investigated. We concluded welding speed and laser power are most significant factors in all process outputs and focal point position has no influence on process outputs in selected ranges. So in this study, the linear heat input (H) was used to assessment the welds, as indicated by Eq. (1):

$$H = \frac{P}{S} \quad (1)$$

Where P is the laser power and S is the laser speed.

The relation between the laser power and the fusion zone area was used to investigate the efficiency of the welding process [8]. The welding process efficiency (E) was presented to consider the amount of energy spent to generate a fusion zone in the work piece. This investigation is very useful because it allows predicting and determining linear heat input value which is necessary to obtain the requested A_{FZ} .

The welding process efficiency (E) was expressed by Eq. (2):

$$E = \frac{A_{FZ}}{H} \quad (2)$$

Where A_{FZ} is the fusion zone area and H is the linear heat input.

Very stable operating conditions are required to maintain a balance between the keyhole-generating forces (gas velocity, vapour pressure and recoil pressure) and the forces tending to close the keyhole (surface tension and gravitational). This balance must be keep for stability the keyhole [21]. The stability of full penetration welding process can be assessed by the ratio of root width to top width (R_w). A stable full penetration welding process for the titanium alloy can be obtained at a weld width ratio of greater than 0.4 [17]. So in this study, the value of 0.4 was selected as evaluation criteria of the weld geometry.

After laser welding, the weld beads were analyzed by X-ray radiographic examination to determine welding defects, according to ASTM E1032. Metallographic and hardness

specimens were cut by wire electrical discharge machining perpendicular to the travel direction. Each transverse section of specimen was mounted and polished by metallographic sandpapers of 240, 400, 600, 800, and 1000 sic grades. Etch solvent with the chemical composition of 2 ml HF+ 10 ml HNO₃+ 88 ml deionized H₂O was employed to reveal the general microstructure of the joints. Laser welding geometrical parameters were measured using an OLYMPUS optical microscope and image analyzer software. The microstructures of the joints were observed using scanning electron microscopy (SEM) equipped with an energy dispersive x-ray spectroscopy (EDS). The tensile strength of joints at room temperature was tested by universal testing machine with a cross-head speed of 1 mm/min, according to ASTM E8M-04 standard. The geometry of tensile specimen and its dimensions were shown in Figure 1. The micro hardness across the weldment was measured by a Vickers micro hardness tester with a load of 100 gr, according to ASTM E384 standard.

3 RESULTS AND DISCUSSION

3.1 Weld Bead appearance

The shape of the melt pool as defined by the keyhole (the liquid-vapour interface), its melting and re-solidification front (the solid-liquid interface) and its surface (the liquid-gas interface) is mainly the result of heat conduction, accompanied by convection caused by the relative motion of the work piece and the laser beam and various melt flow phenomena [22]. The linear heat input has a strong impact on the weld geometry.

The measured weld bead geometry, calculated weld width ratio (R_w) and welding process efficiency value (E) were listed in Table 3. Figure 2 shows the cross section of the some selected samples that have the most difference in linear heat input. The comparison between bead geometry of these samples is more significant for the comprehending of the weld metallurgical properties. A trend to change in the weld geometry from V-shape to hourglass shape is observed with increasing linear heat input. The high welding speed accompanied by

low values of laser powers (lower linear heat input) resulted in the formation of a V-shaped weld geometry and lack of penetration due to an insufficient power density. On the other hand, when the welding speed was low and the laser power was high (higher linear heat input), an excessive melting with subsequent weld pool instability occurred that promoted an hourglass shaped weld geometry. As seen in Figure 2, the pool surface was slightly above the work piece surface because of the expansion of the metal upon heating and melting. Also, there is overfilling in some samples due to insufficient welding speed, longitudinal metal liquid flow and excess of shielding gas flow. These factors affect the motion of the weld pool [23].

The heat generated by absorption is conducted into the metal sheets by thermal conduction accompanied by convection. Continuous wave laser beam causes quasi-steady state conditions. For an established quasi-steady state keyhole during continuous wave laser welding the temperature field is governed by conduction of the absorbed laser beam power (distributed over the keyhole wall) and by convection at the welding speed and accompanying melts pool motion. Convection is dominant heat transfer mode in the weld pool. So, the fluid dynamic of the weld pool determines the bead shape. Surface tension, vapor pressure, volume contraction, gravity and phase transformation (melting and re-solidification, evaporation and condensation, metallurgical phase transformations, or chemical reactions) are the main factors that affect the fluid dynamic [22].

In sample 6, temperatures at the bottom surface are higher than those at the top surface. So, surface tension at the bottom part of the weld pool is lower [23]. The created overheating at the root of the weld pool during the source motion causes clock-wise vortex. This clock-wise vortex tends to the growth of the lower molten region. When linear heat input is high (12.75 J/mm), the exposure time of the liquid material to the laser irradiation increases and more volume of metal melts. So, the loss of energy is increased.

In sample 1, less energy transfer to the material (3.00 J/mm). So, W_{FZ} and A_{FZ} were smaller in comparison with sample 6. With decreasing the laser energy, the keyhole size does not increase. So, counterbalancing between surface tension and recoil forces in the bottom part of the melt wall leads to the formation bead. As seen in Table 2, fully penetrated joints were achieved at linear heat input of greater than 4 J/mm.

The influence of linear heat input on W_{FZ} and A_{FZ} is given in Figure 3. W_{FZ} and A_{FZ} increase with increasing linear heat input. This situation can be explained by the melting of more metal. The R_w values as shown in Figure 3b increase from 0 to 0.58 with increasing linear heat input to 12.75 J/mm. The weld cross section showed a V-shape at low linear heat input up to 4 J/mm and then changed to an hourglass shape with increasing linear heat input. The R_w values at linear heat input of greater than 4 J/mm were above 0.4. This meant that the process was stable above 4 J/mm. Since the R_w dropped below 0.4 at linear heat input of less than 4 J/mm, the process was considered unstable.

The relationship between the linear heat input and welding process efficiency is illustrated in Figure 4, Welding process efficiency increases from 0.17 to 0.3 as linear heat input increases from 2.5 J/mm to 5.79 J/mm. With further increasing linear heat input, Welding process efficiency decreases to 0.24.

Parameters set 8 is optimal compared to the other investigated parameter sets due to highest welding process efficiency ($E=0.43$). This implied that the more percentage of energy converts to increase of weld zone in optimum sample. Also R_w value was above 0.4, meaning that a stable full penetration was obtained under this condition.

Non-destructive tests (Radiographic examination) of the laser welds showed that there are pores in the upper part of three partial penetrated samples (samples 1, 3, and 4). Partial penetrated joints are susceptible to have a higher amount of porosity, because the gas bubbles can only escape from the top surface of the bead. Keyhole collapsing causes to the formation

of porosity in the upper part of the bead. Velocity of keyhole collapsing is higher in the upper part than that in the lower part of the weld pool. Therefore, some of the gases entrap in the upper part of the bead (as seen in Figure 2a).

Porosity formation depends on the linear heat input. With increasing linear heat input, the cooling rate decreases. So, there is more time for gases to escape from the weld pool and the risk of porosity formation reduces. Porosity was not observed at linear heat input of greater than 4 J/mm.

3.2 Microstructure

Figure 5 shows the microstructure of the as-received Ti-6Al-4V. As seen, Ti-6Al-4V alloy consists of intergranular β phase (bcc, body central cubic) dispersed in a domain of equiaxed α phase (hcp, hexagonal close packed).

Thermal cycles during welding process alter the microstructure of Ti-6Al-4V alloy. In Figure 6 transformation region from the weld to base metal is seen. As shown, three different zones are visible.

Linear heat input has significantly effect on the fusion zone microstructure. The rapid cooling rate in the weld pool increases the microstructure evolution from β to α' phase. Therefore, acicular α' phase within prior β grains is observed in fusion zone (Figure 7). Lower linear heat input causes to increase the cooling rate. As a result, finer martensite and prior β grains form in the fusion zone microstructure (Figure 7a). On the other hand, with increasing linear heat input, the cooling rate decreases. This higher linear heat input causes to change the martensitic phase from an acicular like to plate like morphology. Also, the prior β grain size increases because longer time exists for β grain coarsening (Figure 7b). Similar microstructure in fusion zone was observed by Akman et al. [14], Squillace et al. [15], Cao and Jahazi [16], and Casalino et al. [8].

More complex structure is seen in HAZ (Figures 8 and 9). The HAZ can be divided into 2 regions, the HAZ near to fusion zone (where the temperature is above the β transus temperature) and the HAZ far from fusion zone (where the temperature is below the β transus temperature). This temperature for Ti-6Al-4V alloy is approximately 995 °C.

The microstructure in the HAZ alters from a rich α' region (the HAZ near to fusion zone) to a poor α' region (the far HAZ from fusion zone) due to temperature gradient. The HAZ near the fusion zone consists of α' phase and β phase. The microstructure of the HAZ far from fusion zone is different from that of the HAZ near the fusion zone, which is composed of the α' phase, the blocky α phase and the β phase. This trend to change in the microstructure from rich α' region to poor α' region was observed by other researcher [8, 15, and 16].

Elemental analysis of welded samples was performed by EDS spectroscopy. EDS analysis results of three zones (fusion zone, heat affected zone and base metal) were summarized in Table 4. As see, there is a small difference in titanium, aluminum and vanadium contents. The weight percentage of aluminum and titanium decreases from the base metal to fusion zone, whereas the weight percentage of vanadium increases. This phenomenon can be attributed to boiling point of these chemical elements. The boiling point of vanadium, titanium and aluminum is 3407 °C, 3287 °C and 2470 °C, respectively. When temperature during welding reaches above the boiling point of the material, some of alloying elements evaporate. The loss of these elements is dependent on the boiling point of each one. Therefore, the weight percentage of vanadium increases from the base metal to fusion zone because it has highest boiling point. While the weight percentage of titanium and aluminum decreases toward the fusion zone due to lower boiling point.

3.3 Mechanical properties

The quality of a weld is mainly determined by its mechanical properties that describe mechanical behavior under load conditions, standardized in terms of the corresponding fracture mechanics. Fracture behavior and its limits depend on the shape of the weld cross section, on the throat depth, on the metallurgy of the fusion zone and on welding defects [22].

3.3.1 Tensile properties

Tensile testing of the laser welded specimen was performed based on ASTM E8M-04 standard to examine the weld strength. The yield strength, ultimate tensile strength and elongation values were summarize in Table 5. It must be underscored that the tensile test carried out on the original sheet. The base metal demonstrated an ultimate tensile strength of 1045 MPa and an elongation of 12.8%. The ultimate tensile strength of joints ranged from 624 MPa to 1002 MPa whereas the elongation of joints ranged from 3.5% to 10.7%. The lower joint strength compared with the base metal is owing to various reasons such as partial penetration depth, porosity, and geometry defects that affect greatly the tensile strength of laser welds. The tensile strength of optimized specimen is approximately 96% of that of base metal indicating that good quality joint was obtained. This result is in a good agreement with observations by other researcher [13, 15, 16, and 18].

3.3.2 Micro hardness

Micro hardness test was performed on the cross-sections of the weldment in accordance with ASTM E384. The typical micro hardness of the Ti-6Al-4V laser welded specimen is shown in Figure 10. As seen, the fusion zone is the hardest region and the hardness decreases rapidly with increasing distance from the fusion zone. Such behavior can be explained by very high cooling rate in laser welding process. The micro hardness value is approximately uniform in the base metal and fusion zone but this value decreases inside the HAZ from the welded boundary to the HAZ/base metal interface due to the variation of the microstructure

(decrease of the martensitic content). Other researchers reported similar micro hardness profiles [8, 16, and 18].

The influence of linear heat input on the micro hardness values in the fusion zone is given in Figure 11. The micro hardness values in the fusion zone decrease with increasing the linear heat input. When liner energy is increased, the cooling rate is decreased. This phenomenon causes a decrease of martensitic phase formation in the fusion zone. The mean values of micro hardness for base metal, heat affected zone and fusion zone were 330 HV, 350 HV and 440 HV, respectively. The micro hardness value for fusion zone is almost 25% more than HAZ and 32% more than base metal.

4. CONCLUSION

In this study, CO₂ laser butt welding was carried out on Ti-6Al-4V sheets with thickness 1.7 mm. Influence of linear heat input on weld bead geometry, microstructure and mechanical properties was investigated. From this investigation the following results can be concluded:

1. The linear heat input is most significant factor for determining the bead geometry. Fully penetrated joints were achieved at linear heat input of greater than 4 J/mm.
2. Fusion zone consists of acicular α' phase within prior coarse β grains. Increasing linear heat input causes to change the martensitic phase from an acicular like to plate like morphology. Also, the prior β grain size increases because longer time exists for β grain coarsening.
3. A microstructure gradient is observed in the HAZ. The microstructure in the HAZ alters from a rich α' region (the HAZ near to fusion zone) to a poor region (the far HAZ from fusion zone) due to temperature gradient.
4. The micro-hardness values on the weld bead cross-section emphasize an appreciable increase, i.e. fusion zone is almost 25% more than heat affected zone and fusion zone is almost 32% more than base metal. The micro hardness values in the fusion zone decrease

with increasing the linear heat input. This phenomenon can be attributed to decrease of martensitic phase formation in the fusion zone.

5. The ultimate tensile strength of joints ranges from 624 MPa to 1002 MPa whereas the elongation of joints ranges from 3.5% to 10.7%. The lower joint strength compared with the base metal is owing to various reasons such as partial penetration depth, porosity, and geometry defects. The tensile strength of optimized specimen is approximately 96% of that of base metal.

REFERENCES

- [1] Dawes C. (1992). Laser Welding (first edition). Great Abington: Wood head Publishing.
- [2] Donachie M.J. (2000). Titanium a Technical Guide (second edition). Materials Park: ASM international.
- [3] Tsai C.J., Wang L.M. (2014). Improved mechanical properties of Ti–6Al–4V alloy by electron beam welding process plus annealing treatments and its microstructural evolution. *Materials and Design*, 60, 587–598.
- [4] Zhang K., Lei Z., Chen Y., Liu M., Liu Y. (2015). Microstructure characteristics and mechanical properties of laser-TIG hybrid welded dissimilar joints of Ti–22Al–27Nb and TA15. *Optics & Laser Technology*, 73, 139–145.
- [5] Stinville J.C., Bridier F., Ponsen D., Wanjara P., Bocher P. (2015). High and low cycle fatigue behavior of linear friction welded Ti–6Al–4V. *International Journal of Fatigue*, 70, 278–288.
- [6] Romero A., Garcia I., Arenas M.A., Lopez V., Vazquez A. (2015). Ti6Al4V titanium alloy welded using concentrated solar Energy. *Journal of Materials Processing Technology*, 223, 284-291.

- [7] Gao X.L., Zhang L.J., Liu J., Zhang J.X. (2014). Porosity and microstructure in pulsed Nd:YAG laser welded Ti6Al4V sheet. *Journal of Materials Processing Technology*, 214, 1316–1325.
- [8] Casalino G., Mortello M., Campanelli S.L. (2015). Ytterbium fiber laser welding of Ti6Al4V alloy. *Journal of Manufacturing Processing*, 20, 250-256.
- [9] Xu P.q., Li L., Zhang C. (2014). Microstructure characterization of laser welded Ti-6Al-4V fusion zones. *Material Characterization*, 87, 179–185.
- [10] Casalino G., Curcio F., Memola F., Minutolo C. (2005). Investigation on Ti6Al4V laser welding using statistical and Taguchi approaches. *Journal of Materials Processing Technology*, 167, 422–428.
- [11] Xiansheng N., Zhenggan Z., Xiongwei W., Luming L. (2011). The use of Taguchi method to optimize the laser welding of sealing neuro-stimulator. *Optics and Lasers in Engineering*, 49 (3), 297–304.
- [12] Li S., Chen G., Zhou C. (2015). Effects of welding parameters on weld geometry during high-power laser welding of thick plate. *International Journal of Advanced Manufacturing Technology*, 79 (1), 177-182.
- [13] Caiazzo F., Curcio F., Daurelio G., Memola Capece Minutolo F. (2004). Ti6Al4V sheets lap and butt joints carried out by CO₂ laser: mechanical and morphological characterization. *Journal of Materials Processing Technology*, 149, 546–452.
- [14] Akman E., Demir A., Canel T., Sinmazcelik T. (2009). Laser welding of Ti6Al4V titanium alloys. *Journal of Materials Processing Technology*, 209, 3705–3713.
- [15] Squillace A., Prisco U., Ciliberto S., Astarita A. (2012). Effect of welding parameters on morphology and mechanical properties of Ti–6Al–4V laser beam welded butt joints. *Journal of Materials Processing Technology*, 212, 427–436.

- [16] Cao X., Jahazi M. (2009). Effect of welding speed on butt joint quality of Ti–6Al–4V alloy welded using a high-power Nd:YAG laser. *Optics and Lasers in Engineering*, 47, 1231-1241.
- [17] Ahn J., Chen L., Davies C.M., Dear J.P. (2016). Parametric optimization and micro structural analysis on high power Yb-fibre laser welding of Ti–6Al–4V. *Optics and Lasers in Engineering*, 86, 156–171.
- [18] Kashaev N., Ventzke V., Fomichev V., Fomin F., Riekehr S. (2016). Effect of Nd:YAG laser beam welding on weld morphology and mechanical properties of Ti–6Al–4V butt joints and T-joints. *Optics and Lasers in Engineering*, 86, 172–180.
- [19] Khorram A., Ghoreishi M. (2011). CO₂ laser welding of Ti6Al4V alloy and the effect of laser parameters on the weld geometry. *Lasers in Engineering*, 21, 135-148.
- [20] Khorram A., Ghoreishi M., Soleymani Yazdi M.R., Moradi M. (2011). optimization of bead geometry in CO₂ laser welding of Ti6Al4V using response surface methodology. *Scientific Research (Engineering)*, 3, 708-712.
- [21] Norrish J. (2006). *Advanced welding processes: Technologies and process control*. Abington Hall: Wood head publishing.
- [22] Dowden J. (2009). *The Theory of Laser Materials Processing: Heat and Mass Transfer in Modern Technology*. Dordrecht: Springer Science + Business Media B.V.
- [23] Zhang L.J., Zhang J.X., Gumenyuk A., Rethmeier M., Na S.J. (2014). Numerical simulation of full penetration laser welding of thick steel plate with high power high brightness laser. *Journal of Materials Processing Technology*, 214, 1710–1720.

TABLE 1 chemical composition of Ti 6Al 4V alloy (Wt %)

elements	Ti	Al	V	Fe	C	N	H	O
content	balance	6	3.98	0.06	0.08	0.05	0.01	0.20

TABLE 2 Laser parameters used in experiment

Samples	Laser power (KW)	Welding speed (m/min)	Focal point position (mm)
1	1.2	24.0	-0.5
2	1.7	24.0	-0.5
3	2	33.5	-0.5
4	1.4	33.5	-0.5
5	2.2	24.0	-0.5
6	1.7	8.0	-0.5
7	2	14.5	-0.5
8(optimum)	2	24	-0.5

TABLE 3 Measured weld bead geometry and calculated R_w and E

Samples	Linear heat input (J/mm)	P_d (mm)	A_{FZ} (mm ²)	Top W_{FZ} (mm)	Bottom W_{FZ} (mm)	R_w	E(mm ³ /J)
1	3.00	1.23	0.55	1.54	0	0	0.18
2	4.25	1.7	1.08	2.01	0.83	0.41	0.28
3	3.58	1.60	1.03	1.98	0	0	0.27
4	2.50	1.3	0.43	1.10	0	0	0.17
5	5.5	1.7	1.69	2.19	1.02	0.46	0.30
6	12.75	1.7	3.08	2.52	1.47	0.58	0.24
7	8.27	1.7	2.33	2.37	1.16	0.49	0.28
8(optimum)	5	1.7	2.14	1.91	0.81	0.42	0.43

TABLE 4 weight percentage of titanium, aluminum and vanadium in the fusion zone, the heat affected zone and the base metal

Zone	Ti (Wt. %)	Al (Wt. %)	V (Wt. %)
base metal	89.88	5.89	4.23
heat affected zone	89.65	5.68	4.67
fusion zone	89.19	5.25	5.56

TABLE 5 Tensile properties of base metal and welded joints at room temperature

Sample number	Yield strength (MPa)	Ultimate tensile strength (MPa)	Elongation (%)
Base metal	980	1045	12.8%
1	566	624	3.5%
2	681	758	5.3%
3	668	730	5.1%
4	667	733	4.6%
5	781	835	6.68%
6	935	972	8.08%
7	930	965	8.45%
8(Optimum)	960	1002	10.7%

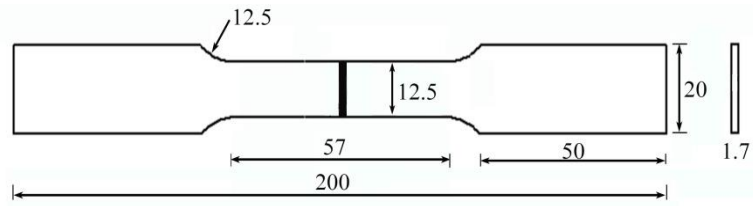
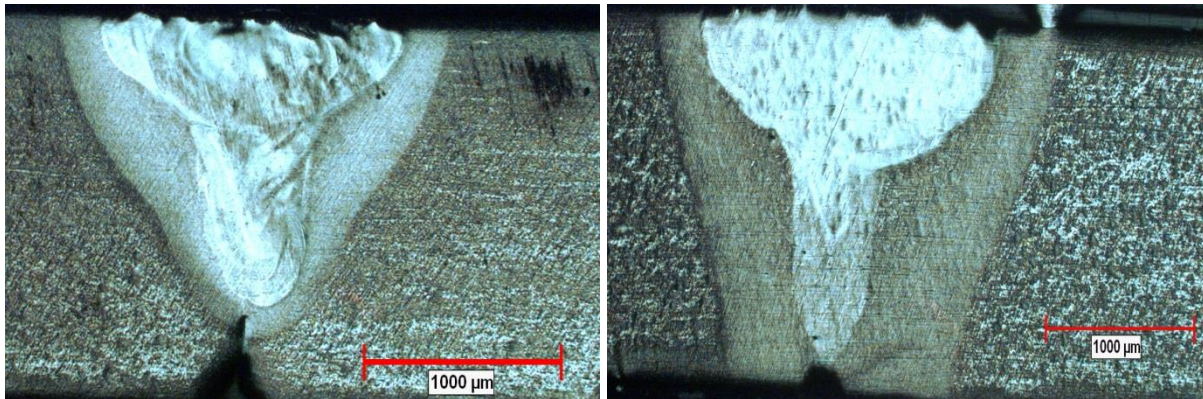
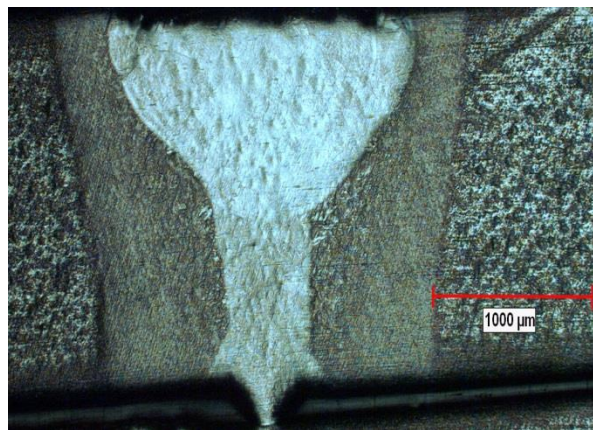


FIGURE 1 Geometry and dimensions (in mm) of a tensile test specimen



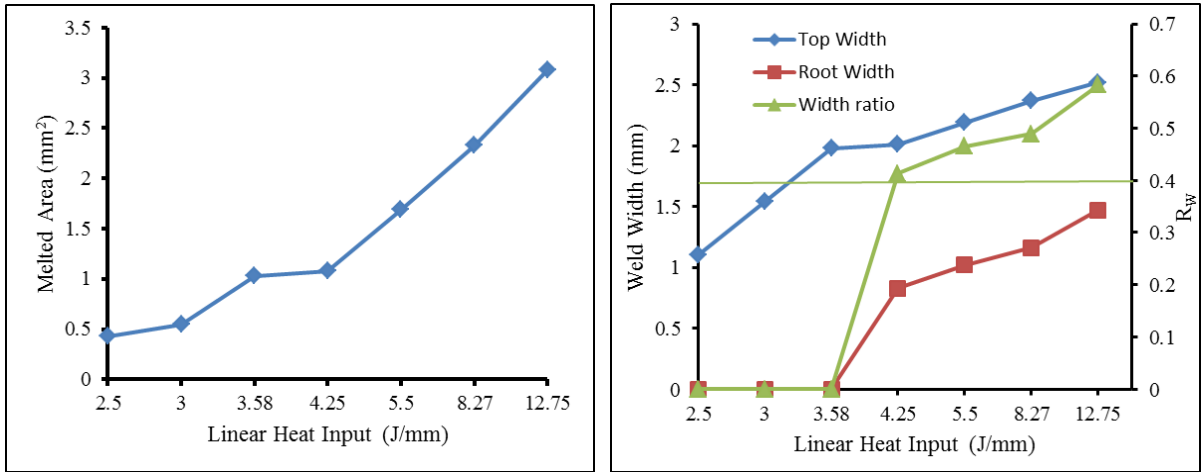
(a)

(b)



(c)

FIGURE 2 Cross section of a) sample 1 ($P= 1.2$ KW, $S=24$ m/min, $F = -0.5$ mm), b) sample 3 ($P= 2$ KW, $S=33.5$ m/min, $F = -0.5$ mm), c) optimum sample ($P= 2$ KW, $S=24$ m/min, $F = -0.5$ mm)



(a)

(b)

FIGURE 3 Relationship between linear heat input and a) A_{FZ} and b) W_{FZ} and weld width ratio (R_w)

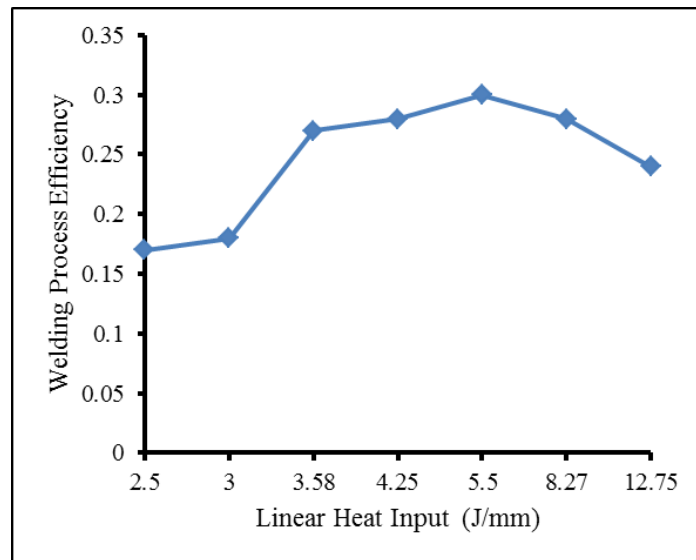


FIGURE 4 Relationship between linear heat input and welding process efficiency

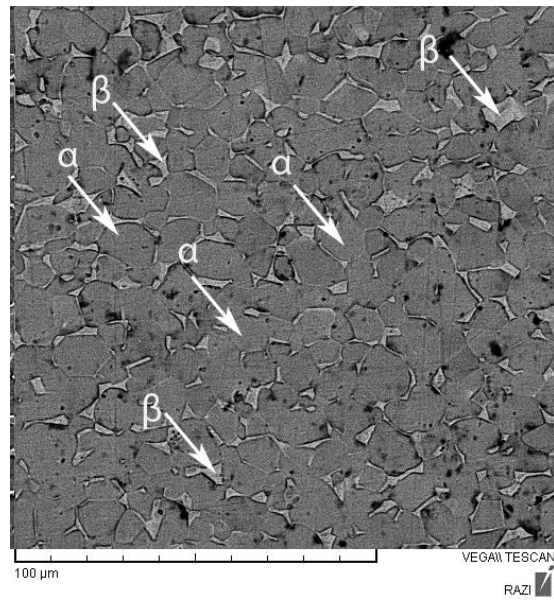


FIGURE 5 Microstructure of base metal

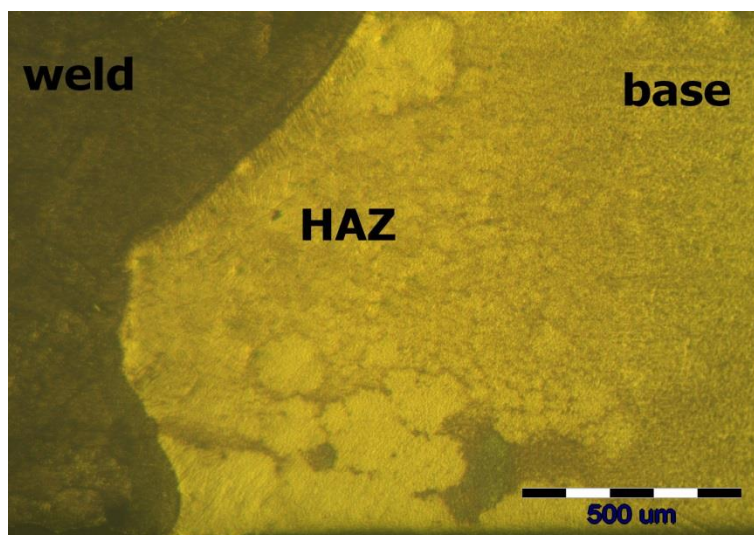


FIGURE 6 Microstructure of combination of base metal, HAZ and fusion zone region

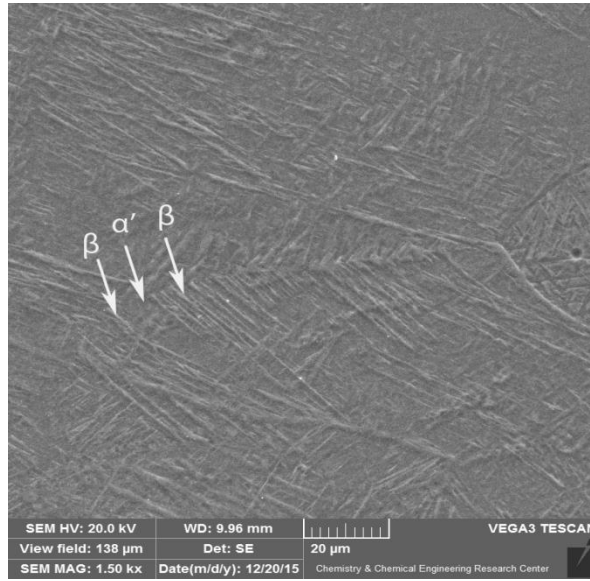


FIGURE 7 Microstructure of fusion zone sample 3 (P= 2 KW, S=33.5 m/min, F = -0.5 mm)

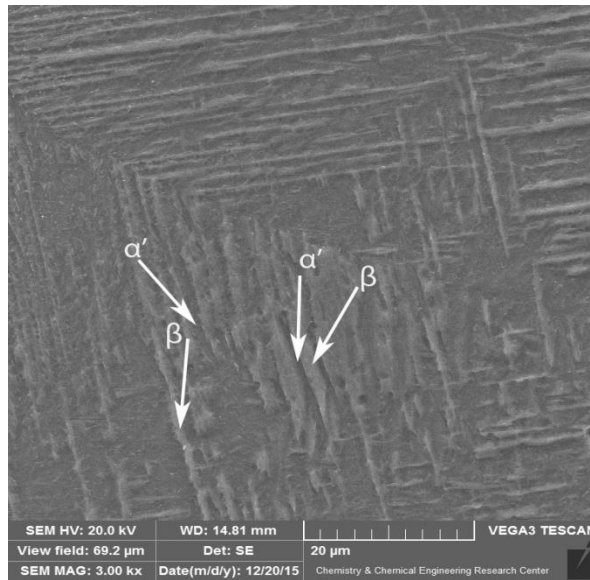


FIGURE 8 Microstructure of HAZ near to fusion zone sample 3 (P= 2 KW, S=33.5 m/min, F = -0.5 mm)

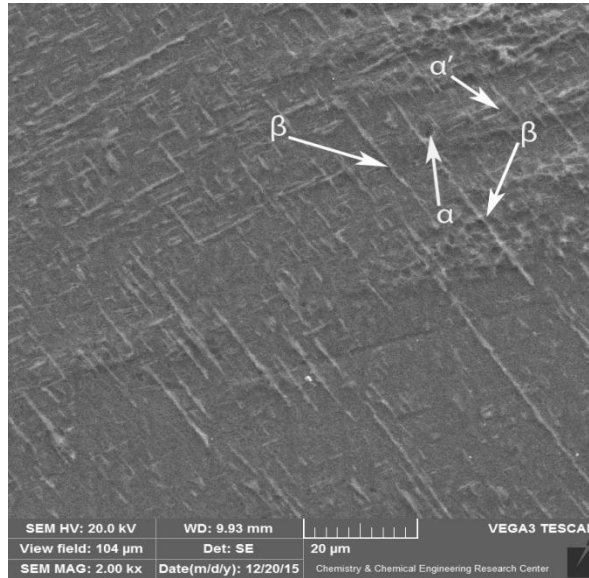


FIGURE 9 Microstructure of HAZ far from fusion zone sample 3 (P= 2 KW, S=33.5 m/min, F = -0.5 mm)

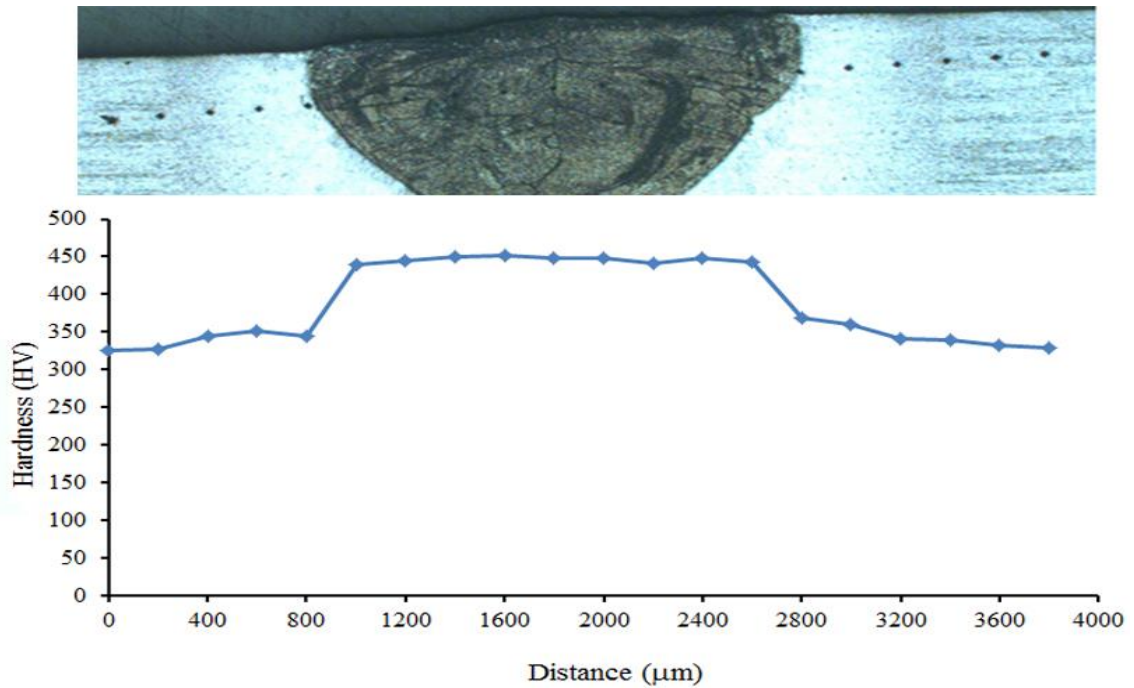


FIGURE 10 The typical micro hardness of the laser welded specimen

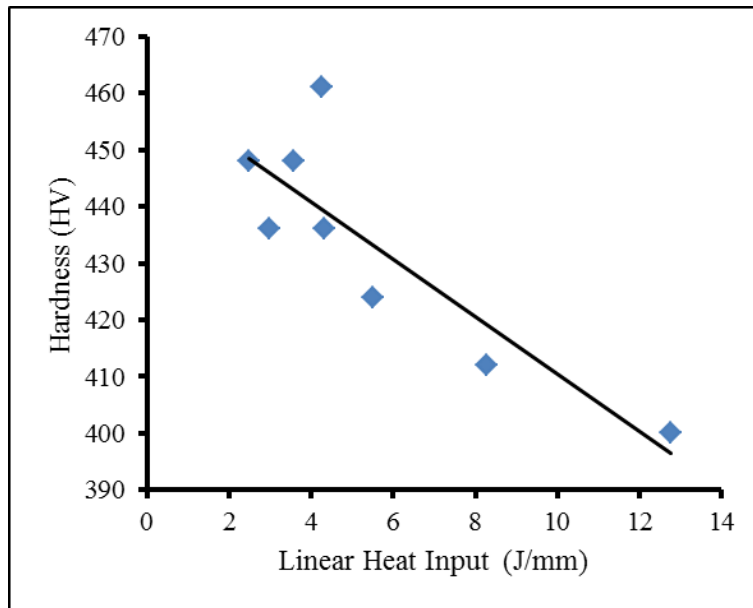


FIGURE 11 Micro-hardness values (HV) versus linear heat input in fusion zone